THE JOURNAL OF BIOLOGICAL CHEMISTRY VOL. 283, NO. 23, pp. 15577–15588, June 6, 2008
Printed in the U.S.A.

New Determinant for the $Ca_V\beta_2$ Subunit Modulation of the $Ca_V1.2$ Calcium Channel*

Received for publication, March 13, 2008 Published, JBC Papers in Press, April 14, 2008, DOI 10.1074/jbc.M802035200

Qi Zong Lao[1], **Evgeny Kobrinsky**[1], **Jo Beth Harry, Arippa Ravindran, and Nikolai M. Soldatov**[2]
From the NIA, National Institutes of Health, Baltimore, Maryland 21224

$Ca_v\beta$ subunits support voltage gating of $Ca_v1.2$ calcium channels and play important role in excitation-contraction coupling. The common central membrane-associated guanylate kinase (MAGUK) region of $Ca_v\beta$ binds to the α-interaction domain (AID) and the IQ motif of the pore-forming α_{1C} subunit, but these two interactions do not explain why the cardiac $Ca_v\beta_2$ subunit splice variants differentially modulate inactivation of Ca^{2+} currents (I_{Ca}). Previously we described $\beta_{2\Delta g}$, a functionally active splice variant of human $Ca_v\beta_2$ lacking MAGUK. By deletion analysis of $\beta_{2\Delta g}$, we have now identified a 41-amino acid C-terminal essential determinant (β_2CED) that stimulates I_{Ca} in the absence of $Ca_v\beta$ subunits and conveys a +20-mV shift in the peak of the I_{Ca}-voltage relationship. The β_2CED is targeted by α_{1C} to the plasma membrane, forms a complex with α_{1C} but does not bind to AID. Electrophysiology and binding studies point to the calmodulin-interacting LA/IQ region in the α_{1C} subunit C terminus as a functionally relevant β_2CED binding site. The β_2CED interacts with LA/IQ in a Ca^{2+}- and calmodulin-independent manner and need LA, but not IQ, to activate the channel. Deletion/mutation analyses indicated that each of the three $Ca_v\beta_2/\alpha_{1C}$ interactions is sufficient to support I_{Ca}. However, β_2CED does not support Ca^{2+}-dependent inactivation, suggesting that interactions of MAGUK with AID and IQ are crucial for Ca^{2+}-induced inactivation. The β_2CED is conserved only in $Ca_v\beta_2$ subunits. Thus, β_2CED constitutes a previously unknown integrative part of the multifactorial mechanism of $Ca_v\beta_2$-subunit differential modulation of the $Ca_v1.2$ calcium channel that in $\beta_{2\Delta g}$ occurs without MAGUK.

Voltage-gated $Ca_v1.2$ calcium channels couple membrane depolarization to excitation in a wide variety of cells. The voltage gating, or membrane potential-dependent opening and closing of a channel, is associated with conformational changes in the pore-forming (α_1) subunit (1). $Ca_v1.2$ channels require auxiliary $\alpha_2\delta$ and β ($Ca_v\beta$) subunits to integrate the functional channel into the plasma membrane (PM)[3] and facilitate voltage gating of the current (2). How $Ca_v\beta$ subunits mediate these functions and what are the $Ca_v\beta$-specific determinants are important questions to be answered. Members of the $Ca_v\beta$ family are structurally divergent. Four different $Ca_v\beta$ subunit genes code for β_1–β_4 subunit variants, some of which are alternatively spliced. Cytosolic $Ca_v\beta$ subunits bind to the 18-amino acid α_1-*i*nteraction *d*omain (AID) of the cytoplasmic linker between internal repeats I and II of the pore-forming α_1 subunit (Fig. 1), stimulate the Ca^{2+} channel current (I_{Ca}), and shift the current-voltage (*I-V*) curve to more negative voltages (3, 4). The AID is conserved between the Ca_v1 and Ca_v2 subfamilies of Ca^{2+} channels. It is located in close proximity to the transmembrane segment IS6 that is a part of the pore domain (5) implicated in voltage-dependent inactivation of the channel (6, 7). A common central region of $Ca_v\beta$ subunits has structural similarity with the membrane-associated guanylate kinase (MAGUK) motif (8). When co-expressed with the α_{1C} subunit, the $Ca_v\beta$ MAGUK domain increased Ba^{2+} current (I_{Ba}) amplitude and shifted the steady-state activation (9). Confirming tight binding of the central $Ca_v\beta$ domain to the α_{1C} subunit, diffraction studies revealed structural patterns that were implicated in interaction with the AID (10–12). However, variant-specific regulatory properties of $Ca_v\beta$ appear to be AID-independent. Although different $Ca_v\beta$ subunits have MAGUK, they modulate Ca^{2+} channels with individual characteristic variations. For example, the primary cardiac β_{2a} subunit did not fully substitute the β_{1a} subunit in skeletal muscle EC coupling although it restored activation of I_{Ca} and gating of Ca^{2+} transients (13). Unlike other $Ca_v\beta$ subunits, β_{2a} endows the distinct cardiac phenotype by not supporting facilitation of the Ca^{2+} channel current by a depolarizing prepulse (14). This general picture was further detailed by FRET microscopy combined with patch clamp that demonstrated differential voltage-dependent rearrangement of $Ca_v\beta$ subunits *vis à vis* the α_{1C} subunit N terminus (15). Unlike the $Ca_v\beta_{1a}$ subunit, $Ca_v\beta_2$ exhibited no such mobility. These and other findings show that a number of $Ca_v\beta$ functions do not rely on AID as a main site of regulation and may involve other determinants (16, 17). Thus, identification of functional motifs that are unique for different $Ca_v\beta$ subunits may give an important insight into the functional specificity of the $Ca_v\beta$-dependent modulation. One feasible approach is to explore the naturally occurring $Ca_v\beta$ splice variants (18). In line with this was the discovery of two new functionally active small

* This work was supported, in whole or in part, by the National Institutes of Health NIA Intramural Research Program. The costs of publication of this article were defrayed in part by the payment of page charges. This article must therefore be hereby marked "*advertisement*" in accordance with 18 U.S.C. Section 1734 solely to indicate this fact.

[1] Both authors contributed equally to this work.

[2] To whom correspondence should be addressed: 5600 Nathan Shock Dr., Baltimore, MD 21224. Tel.: 410-558-8343; Fax: 410-558-8318; E-mail: soldatovN@grc.nia.nih.gov.

[3] The abbreviations used are: PM, plasma membrane; Ab, antibody; AID, α_1-interaction domain; anti-LC, anti-Living Color Ab to EGFP; β_2CED, C-terminal essential determinant of the $Ca_v\beta_2$ subunit; CaM, calmodulin; CDI, Ca^{2+}-dependent inactivation; ECFP, enhanced cyan fluorescent protein; EYFP, enhanced yellow fluorescent protein; IP, immunoprecipitation; MAGUK, membrane-associated guanylate kinase; V_h, holding potential; V_t, test potential; SH, Src homology domain; HEK, human embryonic kidney.

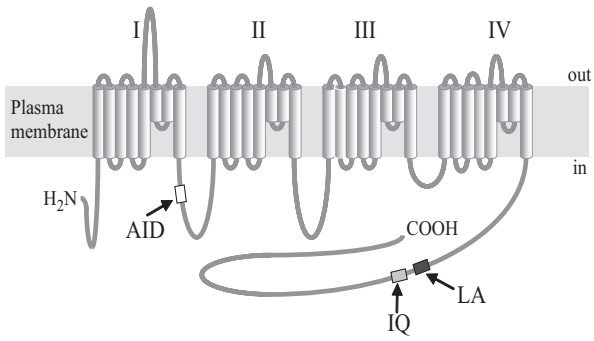

AID: $_{428}$QQLEEDLKGYLDWITQAE$_{445}$

LA: $_{1572}$IKTEGNLEQANEELRAIIKKIWKRTSMKLLDQV$_{1604}$

IQ: $_{1617}$KFYATFLIQEYFRKF$_{1632}$

FIGURE 1. **Transmembrane topology of the α_{1C} subunit showing AID, LA, and IQ motifs and their amino acid sequences in the human α_{1C} protein (below).**

splice variants of the human cardiac β_2 subunit lacking the central domain (19). These β_{2f} and $\beta_{2\Delta g}$ subunits share a 153-amino acid distal C-terminal region common to all known "large" $Ca_v\beta_2$ subunits (β_{2a}–β_{2e}) (20) suggesting that this region may have a role of an essential $Ca_v\beta_2$ determinant. Our attention to this region of the β_2 subunit was stimulated by the finding that $\beta_{2\Delta g}$ supports I_{Ca} on co-expression with α_{1C} and $\alpha_2\delta$ in $Ca_v\beta$-free COS1 cells. Because large and small $Ca_v\beta_2$ splice variants convey sharply different inactivation kinetics, it seems apparent that, in addition to MAGUK, there is a C-terminal determinant (defined here as β_2CED) that is common only to $Ca_v\beta_2$ subunits and thus may contribute to the $Ca_v\beta_2$-specific tuning of the channel modulation by large $Ca_v\beta_2$ subunits. In the case of the small $Ca_v\beta_2$ subunits, β_2CED may play the key regulatory role. This intriguing possibility prompted us to locate β_2CED and characterize the properties of β_2CED-modulated Ca^{2+} channels that rely on β_2CED-dependent, MAGUK-independent modulation.

EXPERIMENTAL PROCEDURES

Molecular Biology, $\beta_{2\Delta g}$ Deletion Mutants—Cloning of β_{2g} (AY675092), subcloning into the pcDNA3 vector, and the 5′-terminal fusion of ECFP have been described previously (19). To create ECFP-labeled $\beta_{2\Delta g}$ deletion mutants, the general strategy was to generate the deletion mutants by PCR and then replace the $\beta_{2\Delta g}$ open reading frame in 5′-ECFP-$\beta_{2\Delta g}$-pcDNA3 with a deletion mutant at the 5′-XhoI/ApaI-3′ sites. The PCR were performed with $\beta_{2\Delta g}$ as template using the following primer pairs with 5′-XhoI linker (sense) and 3′-ApaI-TGA linker (antisense): 5′-cccgctcgagATGTATCTCTGGAGGAGGACC-3′ (sense) and 5′-gcgggcccTCAGTGGTCATGGGAATAATC-3′ (antisense) for $\beta_{2\Delta g}$(1–82); 5′-gcctcgagGTGGACCACTATGCCTCAC-3′ (sense) and 5′-gggcgggcccTCAGTTGTGGTCCTGCTCTCGATC-3′ (antisense) for $\beta_{2\Delta g}$(83–123); 5′-cggcggccgccaccATGGAGTGCAACAAGCAGCGCAGCCGTC-3′ (sense) and 5′-gggcgggcccTCATTGGCGGATGTAAACATG-3′ (antisense) for $\beta_{2\Delta g}$(124–164). To create the deletion mutant 5′-ECFP-$\beta_{2\Delta g}$(83–164)-pcDNA3, 5′-ECFP-$\beta_{2\Delta g}$-pcDNA3 was cut by XhoI, filled-in to a blunt end, cleaved by PmlI, and then the 6.2-kb fragment was self-ligated. To generate the unlabeled $\beta_{2\Delta g}$(124–165), a PCR product was amplified using the NotI linker/Kozak primer (sense) 5′-cggcggccgccaccATGGAGTGCAACAAGCAGCGCAGCCGTC-3′ and the ApaI primer/linker (antisense) 5′-gggcgggcccTCATTGGCGGATGTAAACATG-3′. The $\beta_{2\Delta g}$(124–165) PCR product was subcloned into 5′-ECFP-$\beta_{2\Delta g}$-pcDNA3 or $\beta_{2\Delta g}$-pcDNA3 plasmid at the NotI/ApaI sites (replacing the $\beta_{2\Delta g}$ cassette). To create the mVenus-labeled deletion mutants, the 5′-BsrGI/ApaI-3′ inserts of the ECFP-labeled deletion mutants were subcloned into the mVenus-C1 vector (kindly provided by Dr. S. S. Vogel) cleaved at the same sites.

5′-ECFP-β_{2d}-pcDNA3 was prepared by ligation of the 5′-PshAI/BsmBI-3′ fragment of β_{2b} into the respective sites of plasmid 5′-ECFP-β_{2f}-pcDNA3. The 5′-ECFP-$\beta_{2d\Delta CED}$ deletion construct in pcDNA3 was produced by substitution of 5′-ECFP-β_{2d}-pcDNA3 at the BsmBI-AvrII sites with the respective fragment of $\beta_{2\Delta g}$(83–123)-pcDNA3. The β_{2b} cDNA was amplified by reverse transcriptase-PCR from human heart mRNA with the sense 5′-ATGCTTGACAGACGCCTTATAG-3′ and antisense 5′-GCTGTTAGTTATACAAGACTTC-3′ primers as described earlier (19).

$FLAG_N$-β_{2d} and $FLAG_N$-$\beta_{2d\Delta CED}$ in pcDNA3 were produced by ligating the 5′-BsrGI (filled in with Klenow)/AvrII-3′ fragments of $pECFP_N$-β_{2d} and $pECFP_N$-$\beta_{2d\Delta CED}$, respectively, into a FLAG-2AB-pcDNA3 vector (gift of Dr. Kuanghueih Chen) at the EcoRV and AvrII sites. To prepare $mVenus_N$-β_{2d} and $mVenus_N$-$\beta_{2d\Delta CED}$ in pcDNA3, the 5′-BsrGI/AvrII (filled in with Klenow)-3′ fragments of 5′-ECFP-β_{2d}-pcDNA3 and 5′-ECFP-$\beta_{2d\Delta CED}$-pcDNA3, respectively, were ligated into the mVenus-C1 vector at the BsrGI and EcoRI (filled in with Klenow) sites.

$mVenus_N$-I-II_{AID} was constructed by PCR amplification of the 418–455 fragment of the $\alpha_{1C,77}$ I-II linker (nucleotides 1252–1365 of the pHLCC77 (z34815) open reading frame) in pcDNA3 followed by subcloning into the 5′-BspEI/EcoRI-3′ sites of the mVenus-C1 vector. The sense and antisense primers used were 5′-catatatccggaCGGGGAGATTTCCAGAAG-3′ and 5′-cggcatgaattctaGCCTTCGTCCTCATTC-3′, respectively. $mVenus_N$-I-II_{AIDM} was created in the same way except that $\alpha_{1C,77AIDM}$ was used as the template for PCR. $Biotin_N$-I-II_{AID} in pcDNA6 was prepared with a Zero Blunt TOPO PCR cloning kit (Invitrogen) and a pcDNA^{TM} 6 BioEase Gateway Biotinylation System (Invitrogen) according to the manufacturer's instructions using α_{1C77}-pcDNA3 as template, 5′-cacCATGCGGGAGATTTCCAG-3′ and 5′-ctaGCCTTCGTCCTCATTCTC-3′ as sense and antisense primers, respectively.

To prepare $FLAG_N$-LA/IQ (amino acids 1571–1636 of α_{1C77}) in pcDNA3 vector, PCR was performed with α_{1C77}-pcDNA3 as template, 5′-gtattaaagcttAGGATCAAAACAGAAGGGAACCTAG-3′ and 5′-ctatatgggcccctaCTCTTTGCGCTTCTTGAACTTCC-3′ as sense and antisense primers, respectively; the PCR product was then subcloned into a FLAG-2AB-pcDNA3 vector at the HindIII/ApaI sites. $FLAG_N$-$\alpha_{1C,77}$-pcDNA3 was created by replacement of the

5′-NdeI/HindIII-3′ fragment of α_{1C77}-pcDNA3 with the respective fragment from FLAG-2AB-pcDNA3.

The AID mutant $\alpha_{1C,77AIDM}$ (D433A,G436A,Y437A,W440A) was generated by a "two-step" PCR site-directed mutagenesis. Briefly, two PCR fragments were produced with $\alpha_{1C,77}$-pcDNA3 as template and pairs of outer sense and mutagenesis antisense primers, and mutagenesis sense and outer antisense primers, respectively. The mutagenesis antisense and sense primers contained the desired mutated sequence and had 18 bases complementary to each other. The two fragments were fused together by denaturing, annealing, and *Taq* polymerase extension, the fused DNA product was then amplified by PCR with the outer primer pair. The outer sense and antisense primers were designed from the vector region 5′-ctatagggagacccaagcttc-3′ and $\alpha_{1C,77}$ open reading frame 5′-CACTTCCTTCTGCAGAACCG-3′ (1550 → 1531), respectively; the mutagenesis antisense and sense primers were 5′-ATCCAGGgcGgCTTTGAGAgCCTCTTCTAGC-TGCTGCTT-3′ and 5′-CTCAAAGcCgcCCTGGATgcGA-TCACTCAGGCCGAAGAC-3′, respectively. The final PCR product was cleaved with HindIII and ClaI and substituted for the 5′-HindIII/ClaI-3′ fragment in $\alpha_{1C,77}$-pcDNA3 resulting in $\alpha_{1C,77AIDM}$-pcDNA3. To produce $mVenus_N$-$\alpha_{1C,77AIDM}$-pcDNA3, the 5′-NdeI/KpnI-3′ fragment of $\alpha_{1C,77AIDM}$-pcDNA3 was replaced with the 5′-NdeI/KpnI-3′ fragment of vector *p*mVenus-C1, which contains the mVenus cDNA and is in a continuous reading frame with $\alpha_{1C,77AIDM}$-pcDNA3.

77ΔLK-pcDNA3 coding for $\alpha_{1C,77\Delta LK}$ was prepared by a similar mutagenesis strategy using pHLCC77 plasmid (21) as a template. The mutagenesis primers were 5′-CAGGGCCTTG-TGGGCAAGCCC-3′ (sense) and 5′-gcccacaaggccctgCAGG-GCCGTCCTGACCAGGGC-3′ (antisense); the outer primers were 5′-CTGTGATGCATGGAATACATTTGACGCCTTG-ATTG-3′ (sense) and 5′-ctagaactagtggatcctctaGAGTC-GACCTGCAG-3′ (antisense). The final PCR product was cleaved with NsiI and XbaI, and then incorporated at the 5′-NsiI and 3′-XbaI sites into pHLCC77. Subsequently, the 5′-PpuMI/XbaI-3′ fragment of the resulting plasmid was ligated at the respective sites in α_{1C77}-pcDNA3. For $\alpha_{1C,77AIDM/\Delta LK}$-pcDNA3, the 5′-PpuMI/XbaI-3′ fragment of $\alpha_{1C,77\Delta LK}$-pCDNA3 was subcloned into $\alpha_{1C,77AIDM}$-pcDNA3. All cDNA constructs were verified by nucleotide sequencing.

Immunoprecipitation Analysis—Human embryonic kidney (HEK) 293 cells were used for the IP analysis because of high expression efficiency. To exclude endogenous $Ca_v1.2$ subunits from the analysis, we expressed only tagged subunits and used antibodies against the tags. For IP-Western blot analysis, ≈80% confluent early passage HEK293 cells in 100-mm culture dishes were transfected with selected plasmids (for details, see figure legends) using Effectene (Qiagen) according to the manufacturer's instructions. 72 h after transfection, cells were harvested and washed 3 times with phosphate-buffered saline. To improve the yield and stability of co-IP, cells were subjected to a standard cross-linking reaction (22, 23) by incubation with the cell-permeant thiol-cleavable reagent dithiobis(succinimidyl propionate) (1 mM) (Pierce) at room temperature for 30 min. Cross-linking was stopped by incubation of cells with 20

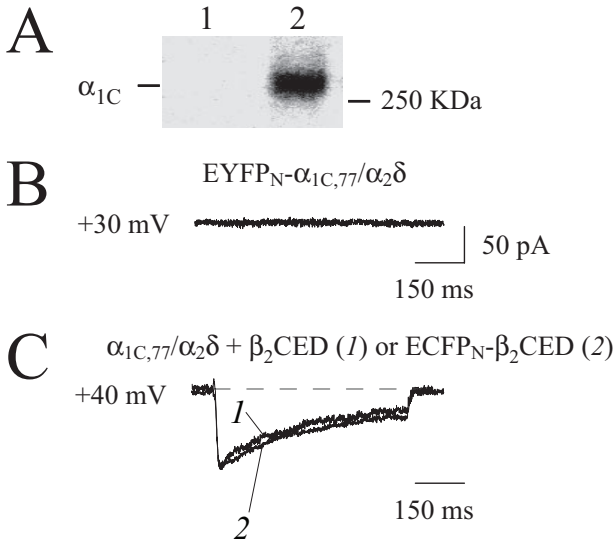

FIGURE 2. **Characterization of expression of Ca^{2+} channels in COS1 cells.** *A*, endogenous α_{1C} subunits are not detectable in COS1 cells by Western blotting. *Lane 1*, non-transfected COS1 cells. *Lane 2*, COS1 cells expressing the recombinant $\alpha_{1C,77}/\alpha_2\delta/\beta_{2d}$ channel. Immunoblot analysis was carried out with antibody against α_{1C} (Chemicon). The position of the α_{1C} subunit is marked on the *left side*; molecular mass (in kDa) is shown on the *right side*. *B*, representative trace of I_{Ca} generated in response to $V_t = +30$-mV applied from $V_h = -90$ mV to COS1 cells transfected by $EYFP_N$-$\alpha_{1C,77}$ and $\alpha_2\delta$ subunits in the absence of $Ca_v\beta$ subunits. No current was observed between 0 and +50 mV. *C*, superimposed traces of the maximal I_{Ca} through the $EYFP_N$-$\alpha_{1C,77}/\alpha_2\delta$ channel with β_2CED (*trace 1*) or $ECFP_N$-β_2CED (*trace 2*) recorded at $V_t = +40$ mV and normalized to the same amplitude. The α_{1C}, $\alpha_2\delta$, and β_2CED subunits were co-expressed in a 1:1:1 molar ratio. No significant difference in the kinetics of the currents was observed.

mM Tris-HCl (pH 7.5) for 15 min. Cells were lysed with a Cel-Lytic M lysis reagent (450 μl/plate, Sigma) containing a protease inhibitor mixture (Sigma, 1/100 dilution) supplemented with 1 mM phenylmethylsulfonyl fluoride. To ensure direct interaction, the microsomal fraction was used for co-IP experiments involving α_{1C}. The 80-μl aliquots of total lysates were kept to verify the expression of each protein (see "input" on immunoblots). Co-IP was performed with the selected antibodies according to the manufacturer's instructions. Briefly, co-IP with anti-FLAG antibody (Ab) was performed with 40 μl/reaction of a monoclonal EZ View™ ANTI-FLAG® M2 affinity gel (Sigma) at 4 °C overnight, and the immunoprecipitates were eluted by incubation with 10 μg of 3× FLAG peptide (Sigma) in 100 μl of TBS solution (pH 7.4) at 4 °C for 1 h. The co-IP with anti-LC Ab was performed with 5 μl of a Living Colors Full-Length A.V. polyclonal Ab (Clontech) using Protein A-agarose (Sigma) as carrier (overnight at 4 °C), and the immunoprecipitates were eluted by boiling for 5 min at 95 °C. Dithiobis(succinimidyl propionate) was cleaved by incubation of the co-immunoprecipitate and input samples with 5% β-mercaptoethanol at 100 °C for 5 min or with 50 mM dithiothreitol at 37 °C for 30 min (only for α_{1C}) before SDS-PAGE. SDS-PAGE and immunoblotting with the indicated antibodies were performed according to standard protocols. The following primary antibodies were used: anti-FLAG M2 monoclonal Ab (2 μg/ml, Sigma) for the FLAG-tagged proteins, Living Colors Full-Length A.V. monoclonal Ab (0.5 μg/ml, Clontech) for the fluorescent tagged proteins, and streptavidin-horseradish peroxi-

dase (1/1000 dilution, Invitrogen) for the biotin-tagged proteins. Nitrocellulose membrane (Invitrogen) was used for immunoblot analysis of α_{1C} co-IP experiments and polyvinylidene difluoride membrane (Invitrogen) was used for all other studies.

Electrophysiology—The Effectene kit (Qiagen) was used for transfection of COS1 cells as described previously (15) under conditions optimized for a total amount of 0.2 μg of DNA per 35-mm Petri dish. Constructs were expressed in a 1:1 molar ratio. COS1 cells were grown on poly-D-lysine-coated coverslips (MatTek) in Dulbecco's modified Eagle's medium supplemented with 10% fetal calf serum. Whole-cell patch clamp recordings were performed as described (24) at 20–22 °C using the Axopatch 200B amplifier (Axon Instruments) 48–72 h after transfection. The extracellular bath solution contained (in mM): 100 NaCl, 20 $BaCl_2$ or $CaCl_2$, 1 $MgCl_2$, 10 glucose, 10 HEPES, adjusted to pH 7.4 with NaOH. Borosilicate glass pipettes (Kimax-51, Kimble Products) were fire-polished and showed a typical resistance of 3–6 megohms when filled with pipette solution containing (in mM): 110 CsCl, 5 MgATP, 10 1,2-bis(2-aminophenoxy)ethane-*N*,*N*,*N*′,*N*′-tetraacetic acid, 20 tetraethylammonium, 0.2 cAMP, and 20 HEPES, adjusted to pH 7.4 with CsOH (15). Voltage protocols were generated and data were digitized, recorded, and analyzed using pClamp 8.1 software (Axon Instruments). Test pulses were applied at 15-s intervals from the holding potential $V_h = -90$ mV. Currents were filtered at 1 kHz, sampled at 2.5–5 kHz, and corrected for leakage using an on-line P/4 subtraction protocol. At the end of experiments, channels were routinely tested for sensitivity of I_{Ca} to the inhibition by the dihydropyridine blocker PN200-110 (see examples). *I-V* curves were obtained by step depolarization to test potentials in the range of −60 to +90 mV (with 10-mV increments) applied from V_h. Steady-state inactivation curves were measured with conditioning pulses (1 s) applied from $V_h = -90$ mV up to −60 to +40 mV with 10-mV increments followed by a 100-ms test pulse. Peak current amplitudes were normalized to the maximal value. Averaged *I-V* curves

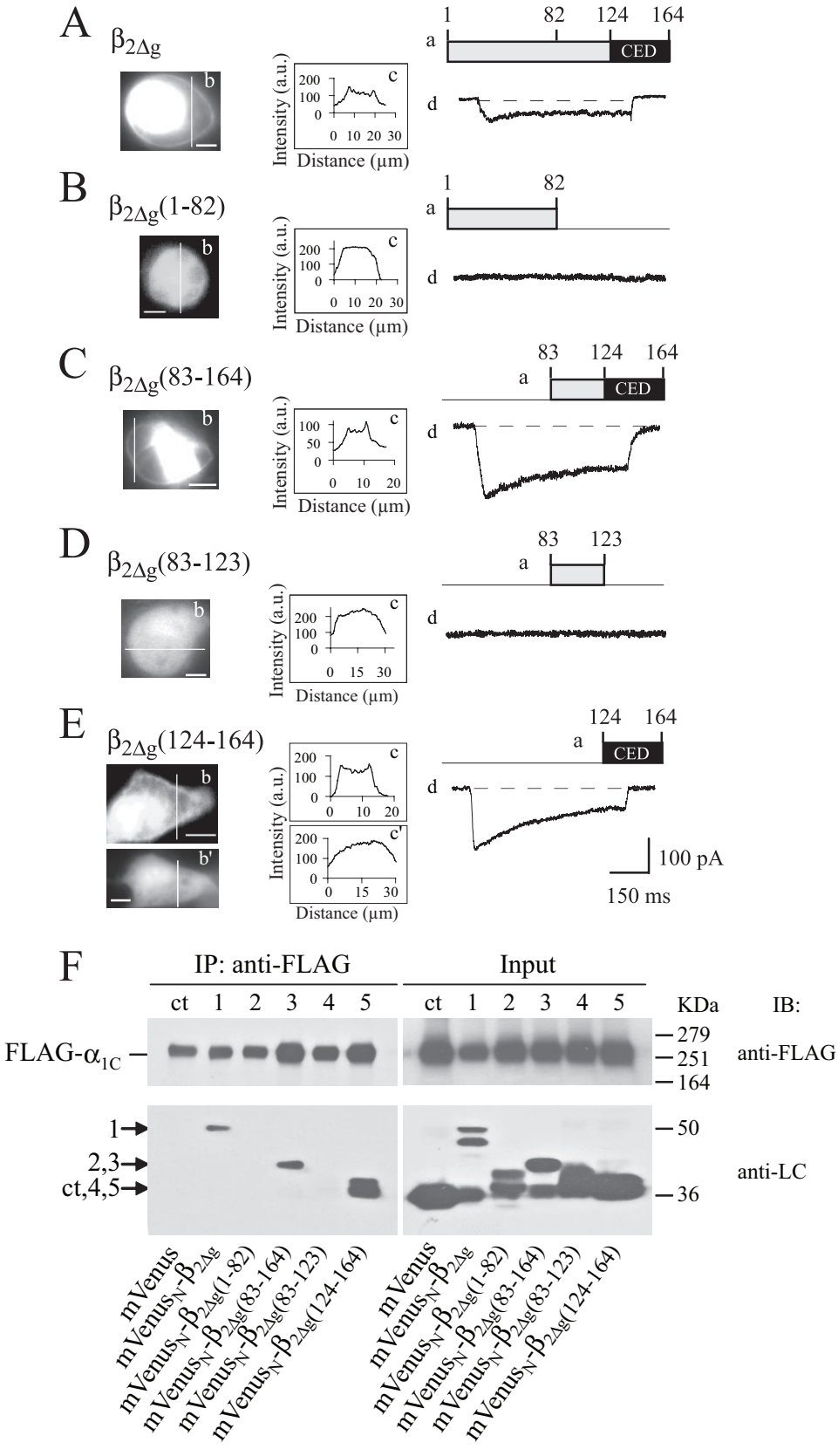

were fit with the equation: $I = G_{max}\ (V - E_{rev})/(1 + exp[(V - V_{0.5,act})/k_{I\text{-}V}])$, where G_{max} is maximum conductance, E_{rev} is reversal potential, $V_{0.5,act}$ the voltage at 50% of the current (I) activation, and $k_{I\text{-}V}$ the slope factor. Steady-state inactivation curves were fitted by a Boltzmann function: $I = a + b\cdot(1 + exp[(V - V_{0.5,in})/k_i])$, where V is the conditioning pulse voltage; $V_{0.5,in}$ is the voltage at half-maximum of inactivation, k_i is a slope factor, a and b are fractions of noninactivating and inactivating components of the current, respectively. To estimate the time constant τ of inactivation, currents were fitted with the Chebyshev method according to the standard exponential function,

$$I(t) = \sum_{i=1}^{n} I_i e^{-t/\tau_i} + I_0 \qquad \text{(Eq. 1)}$$

where I_i is the amplitude of the inactivating component of the current, τ is the time constant of inactivation, and I_0 is the non-inactivating component of the current. Statistical values are given as mean ± S.E. Error bars in the figures are S.E., *n,* number of tested cells. Differences were considered significant if Student's t test showed $p < 0.05$.

Imaging—Cell images were recorded with a 14-bit Hamamatsu digital camera C9100-12 mounted on the Nikon epifluorescent microscope TE200 (60 × 1.2 N.A. objective) equipped with multiple filter sets (Chroma Technology, Rockingham, VT). Excitation light was delivered by a 175-watt Xenon lamp. Images were obtained and analyzed using C-Imaging software program (Compix, Sewickley, PA).

RESULTS

Selection of Appropriate Expression System—Electrophysiological studies of Ca^{2+} channels are traditionally based on the use of HEK293 cells. However, several independent careful evaluations have shown that these cells contain endogenous Ca^{2+} channel subunits and exhibit I_{Ca} at a level of 1–3 pA/pF (25, 26). Thus, HEK293 cells can be used safely for the functional analysis of recombinant Ca^{2+} channels only when the amplitude of the current is large enough to ignore the contribution of the endogenous channels. To avoid this problem, in this study we used COS1 cells because they lack endogenous $Ca_v1.2$ subunits (27): (*a*) Western blot analysis with anti-α_{1C} Ab revealed no detectable endogenous α_{1C} in non-transfected COS1 cells (Fig. 2*A*, *lane 1*), and (*b*) no Ca^{2+} channel activity was observed in COS1 cells expressing recombinant α_{1C} and $\alpha_2\delta$ subunits (Fig. 2*B*) in contrast to cells that were co-transfected with β_{2d}, $\beta_{2\Delta g}$, or β_2CED (see below). This experiment unambiguously shows that $Ca_v1.2$ calcium channels are silent in the absence of $Ca_v\beta$ and that activity of the Ca^{2+} channel demonstrated in HEK293 cells in the absence of exogenous $Ca_v\beta$ subunits may be due to endogenous channels. The absence of the functional $Ca_v\beta$ subunits in COS1 cells that follows from the data in Fig. 2*B* was further confirmed by co-IP analysis with recombinant $FLAG_N$-$\alpha_{1C}/\alpha_2\delta$ that revealed a lack of detectable endogenous monkey β_1, β_2, β_3, and β_4 subunits in COS1 cells (28). Kinetics parameters and voltage dependence of activation and inactivation of I_{Ca} and I_{Ba} through the $\alpha_{1C,77}/\alpha_2\delta/\beta_{1a}$ channel measured in COS1 cells were consistent with data obtained in other expression systems (15). An important advantage of COS1 cells is their relatively slow division rate that allows for better control over efficiency of expression and assembly of the $Ca_v1.2$ channel subunits of different size. However, HEK293 cells were more appropriate for co-IP-Western blot analysis of the recombinant tagged channel proteins in our study because they provide higher efficiency of expression, whereas endogenous subunits were undetectable with streptavidin and Abs to FLAG and Venus (ECFP) tags by Western blot analysis and fluorescence microscopy.

Localization of β_2CED by Deletion Analysis of the $\beta_{2\Delta g}$ Subunit—To locate β_2CED, we constructed the following $\beta_{2\Delta g}$ fragments: 1–82, 83–164, 83–123, and 124–164 (Fig. 3, *A–E*, *panels a*). To ease IP and detection, $\beta_{2\Delta g}$ fragments were tagged at the N termini with the monomeric m*Venus* protein (29) or ECFP. As with other $Ca_v\beta$ subunits (*e.g.* β_{1a}, β_{2a} (15), β_{2f} or $\beta_{2\Delta g}$ (19)), fusion of ECFP and mVenus to the N termini of the $\beta_{2\Delta g}$ fragments did not markedly change electrophysiological properties of the expressed channels (*e.g.* β_{2d}(124–164) in Fig. 2*C*). The $ECFP_N$-labeled $\beta_{2\Delta g}$ fragments were co-expressed with the $\alpha_{1C,77}$ and $\alpha_2\delta$ subunits in COS1 cells. The relative tendency of the $ECFP_N$-$\beta_{2\Delta g}$ deletion mutants to accumulate in PM can be seen in close juxtaposition from distribution of ECFP fluorescence in the expressing cells (Fig. 3, *A–E*, *panels b* and *c*). Ability of the $\beta_{2\Delta g}$ deletion mutants to support I_{Ca} was assayed by patch clamp (Fig. 3, *A–E*, *panels d*). Binding to α_{1C} was assayed by co-IP of the $mVenus_N$-labeled $\beta_{2\Delta g}$ fragments with $FLAG_N$-$\alpha_{1C,77}/\alpha_2\delta$ (Fig. 3*F*).

Confirming previous observations (19), when co-expressed with $\alpha_{1C,77}$ and $\alpha_2\delta$ subunits, $\beta_{2\Delta g}$ was appreciably accumulated in PM (Fig. 3*A*, *panels b* and *c*), stimulated inward I_{Ca} with an average maximal amplitude of 80 ± 15 pA ($n = 45$; Fig. 3*A*, *panel d*), and co-immunoprecipitated with α_{1C} subunit (Fig. 3*F*, *lane 1*). Sequential deletion of the $\beta_{2\Delta g}$ subunit (Fig. 3, *B–E*) revealed that calcium channel activity is associated with the distal quarter of the $\beta_{2\Delta g}$ sequence. Only the $\beta_{2\Delta g}$ fragments containing the distal C-terminal regions 83–164 (Fig. 3*C*) and 124–164 (Fig. 3*E*) induced the current when co-expressed with

FIGURE 3. **Localization of β_2CED by deletion analysis of $\beta_{2\Delta g}$.** *A*, $\beta_{2\Delta g}$. *B*, $\beta_{2\Delta g}$(1–82). *C*, $\beta_{2\Delta g}$(83–164). *D*, $\beta_{2\Delta g}$(83–123). *E*, $\beta_{2\Delta g}$(124–164). Shown on the panels are: *a*, scheme of the generated fragments (amino acid numbers are indicated in *A*); *black box*, β_2CED. *b*, whole cell fluorescent images of COS1 cells expressing $\alpha_{1C,77}$ and $\alpha_2\delta$ with the $ECFP_N$-$\beta_{2\Delta g}$ fragments (*scale bars*, 8 μm). In the experiment shown on *E, panel b'*, β_2CED was expressed alone. *c,* intensity profiles of ECFP fluorescence along the scan lines presented on *panels b* and showing PM targeting of the $\beta_{2\Delta g}$ fragments. The fluorescence profile on *panel c'* (*E*) corresponds to *panel b'* (*E*) illustrating lack of membrane targeting by β_2CED in the absence of α_{1C} and $\alpha_2\delta$. *d*, traces of the maximal I_{Ca} evoked by a stepwise depolarization from $V_h = -90$ mV to $V_t = +50$ ($\beta_{2\Delta g}$) or +40 mV (all other constructs). *F*, Western blot analysis of co-IP of $FLAG_N$-$\alpha_{1C,77}$ with $mVenus_N$-labeled $\beta_{2\Delta g}$ (*lane 1*) and its $mVenus_N$-labeled deletion mutants $\beta_{2\Delta g}$(1–82) (*lane 2*), $\beta_{2\Delta g}$(83–164) (*lane 3*), $\beta_{2\Delta g}$(83–123) (*lane 4*), and $\beta_{2\Delta g}$(124–164) (*lane 5*). mVenus (*lane ct*) is the control to confirm the absence of nonspecific binding between the tags. *IP* and immunoblotting (*IB*) were performed with the indicated antibodies as described under "Experimental Procedures." The *Input* panel is the pre-IP immunoblot showing expression of each tagged protein. *Arrows* (*left panel*) mark the location of an mVenus-tagged fragment in each lane. Molecular mass standards (in kDa) are indicated on the *right*.

β_2CED	ECNKQRSRHKSKDRYC-EKDGEVISKKRNEAGEWNRDVYIRQ	41
β_{1b2}	ELTDNRNRGRNKARYCAEGGGPVLGRNKNELEGWGRGVYIR-	596
β_{1b1}	SKHIIIERSNTRSSLA-EVQSEIERIFELARTLQLVALDADT	325
β_3	SGLPSANGHDPQDRLLA-QDSE---HNHSDR-NWQRNRPWPK	481
β_4	RLIKSRGKSQSKHLNV-QLVAADKLAQCPPEMFDVILDENQL	384

FIGURE 4. **Homology alignment of β_2CED with human Ca$_V\beta$ subunits.** Conserved residues are shown in *black boxes*. Blast analysis revealed that β_2CED is 100% conserved in the C termini of all known human Ca$_v\beta_2$ subunits (not shown), whereas only β_{1b2} (M92303) shows 43% of homology with β_2CED. No substantial homology was seen with β_{1b1} (M92302), β_3 (X76555), β_4 (U95020), β_{1a} (not shown), or other human proteins as revealed by a general blast analysis. Thus, β_2CED is unique for Ca$_v\beta_2$ subunits.

$\alpha_{1C,77}/\alpha_2\delta$ (*panels d*) and directly interacted with α_{1C}, as evident from the marked accumulation in PM (*panels b* and *c*) and Western blot analysis of co-IP with microsomal α_{1C} (Fig. 3*F*, *lanes 3* and *5*). Taken together, results of this analysis show that the C-terminal sequence of 41 amino acids of the Ca$_v\beta_2$ subunit (β_2CED) represents a previously unknown determinant that may have a role in calcium channel modulation. Amino acid alignment revealed (Fig. 4) that β_2CED is conserved in Ca$_v\beta_2$ and shares only a subtle homology with the other Ca$_v\beta$ subunits.

Electrophysiological Properties of the β_2CED-supported Channel—In COS1 cells expressing EYFP$_N$-$\alpha_{1C,77}$ and $\alpha_2\delta$ subunits, the average maximal amplitude of I_{Ca} decreased from 647 ± 34 pA (n = 48) with β_{2d} to 120 ± 25 pA (n = 48) with β_2CED. Fig. 5*A* shows a family of representative traces of I_{Ca} evoked by a stepwise depolarization in the range of −20 to +60 mV applied from V_h = −90 mV. The currents were almost completely inhibited by the specific L-type calcium channel blocker (+)PN200-110 (Fig. 5*B*, *traces a*). An interesting feature of these currents is the presence of a large slow component of inactivation that is unusual for the Ca^{2+}-conducting Ca$_v$1.2 channels. Analysis of the steady-state inactivation curve (Fig. 5*C*) showed that at the end of a 1-s conditioning pulse 14.5 ± 1.7% (n = 12) of the peak I_{Ca} remained non-inactivated. Analysis of ~50 expressing cells revealed that I_{Ca} evoked by V_t between −20 and 0 mV are better fitted with two exponentials and showed a prominent fast component of inactivation (see Table 1). The latter property can be better appreciated from the exemplar I_{Ca} traces (recorded at −20 and −10 mV) in Fig. 5*B* that have larger amplitude than the representative currents in Fig. 5*A*. However, at $V_t \geq$ 10 mV, the decay of I_{Ca} was better fitted by a single exponential. The large sustained current (I_0, Table 1) is characteristic for all shown voltages and may be indicative of the inhibited slow inactivation (6, 24).

Co-plotting of *I-V* and *τ-V* curves (Fig. 5*D*) showed that when β_{2d} in the channel (Table 1) was replaced with β_2CED, inactivation of I_{Ca} became slower on stronger depolarization and did not depend on the size of the current. The corresponding lack of U-shaped *τ-V* dependence is evidence that β_2CED does not support CDI (30). To further characterize modulation of inactivation of the Ca$_v$1.2 channel by β_2CED, we tested the effect of replacement of Ca^{2+} for Ba^{2+} in the bath medium on kinetics of the current decay. When Ba^{2+} is the charge carrier, Ca$_v$1.2 channels inactivate by a voltage-dependent mechanism (2). The *I-V* relationship for I_{Ba} ($V_{0.5,act}$ = 41.3 ± 4.3, n = 31, Fig. 5*E*) was shifted to more positive potentials as compared with I_{Ca} ($V_{0.5,act}$ = 19.8 ± 1.8, n = 48, Fig. 5*D*). A ~10-mV positive shift of the steady-state inactivation curve was also observed on replacement of Ca^{2+} ($V_{0.5,in}$ = 13.9 ± 1.1) for Ba^{2+} ($V_{0.5,in}$ = 24.2 ± 3.3) in the bath medium (Fig. 5*C*), whereas the voltage dependence of availability of the β_2CED-modulated channel was increased to 50.6 ± 2.9% (n = 24) with Ba^{2+} as the charge carrier. These data suggest that the inactivating fraction of channels is reduced in Ba^{2+} because of increased voltage dependence of availability of the β_2CED channel.

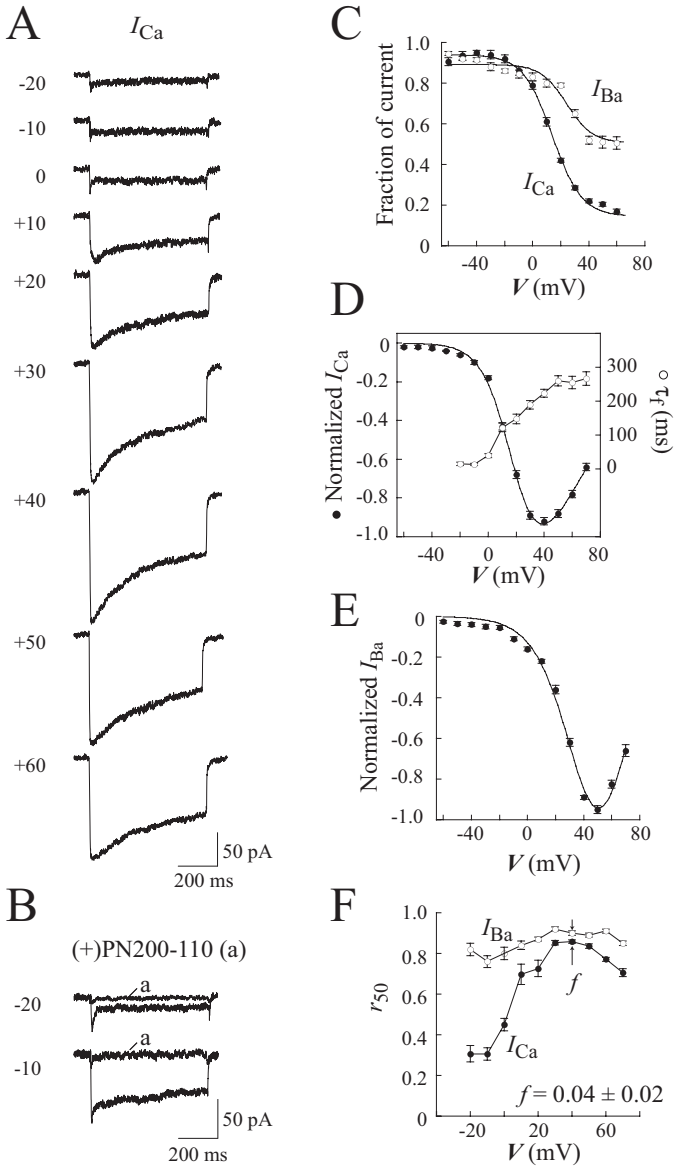

FIGURE 5. **Electrophysiological properties of the β_2CED-modulated calcium channel.** *A*, representative traces of I_{Ca} evoked by the indicated test pulses applied for 600 ms from V_h = −90 mV. β_2CED was co-expressed in COS1 cells with EYFP$_N$-$\alpha_{1C,77}$ and $\alpha_2\delta$ subunits. *B*, exemplar recordings of I_{Ca} before and after (*traces a*) application of 4 μM (+)PN200–110. Values of V_t are shown on the *left*. *C*, steady-state inactivation curves for I_{Ca} (n = 12) and I_{Ba} (n = 24). *D*, the normalized *I-V* curve (*filled circles*) and voltage dependence of τ_f (*open circles*) for I_{Ca}. See text for $V_{0.5,act}$ statistics (n = 48). *E*, the normalized *I-V* relationship for I_{Ba} (n = 31). *F*, dependence of r_{50} on test pulse voltage for I_{Ca} (*filled circles*, n = 48) and I_{Ba} (*open circles*, n = 31). Factor *f* is the difference between the r_{50} values of I_{Ca} and I_{Ba} at the maximum of *I-V* curves (+40 mV). *Smooth lines* in *C–E* represent fits of the average data (see "Experimental Procedures").

TABLE 1
Comparison of kinetics parameters of inactivation of I_{Ca} through the $Ca_v1.2$ channel modulated by β_{2d} and β_2CED

V	β_{2d} ($n = 48$)					β_2CED ($n = 48$)				
	I_0	I_f	τ_f	I_s[a]	τ_s	I_0	I_f	τ_f	I_s[b]	τ_s
mV			*ms*		*ms*			*ms*		*ms*
−20						0.50 ± 0.03	0.32 ± 0.02	15 ± 5	0.27 ± 0.03	118 ± 30
−10	0.49 ± 0.13	0.52 ± 0.10	284 ± 10[c]			0.47 ± 0.03	0.39 ± 0.03	13 ± 3	0.25 ± 0.04	142 ± 39
0	0.59 ± 0.04	0.42 ± 0.04	132 ± 20[c]			0.57 ± 0.03	0.35 ± 0.04	40 ± 6	0.05 ± 0.02	180 ± 26
10	0.46 ± 0.03	0.43 ± 0.02	86 ± 13	0.10 ± 0.02	310 ± 75	0.47 ± 0.03	0.49 ± 0.04	122 ± 12		
20	0.34 ± 0.03	0.47 ± 0.02	59 ± 6[c]	0.19 ± 0.02	388 ± 63	0.43 ± 0.02	0.57 ± 0.03	148 ± 14		
30	0.33 ± 0.02	0.55 ± 0.02	96 ± 6[c]	0.12 ± 0.02	485 ± 62	0.36 ± 0.01	0.64 ± 0.03	189 ± 12		
40	0.31 ± 0.02	0.67 ± 0.02	119 ± 7[c]			0.37 ± 0.01	0.63 ± 0.03	223 ± 12		
50	0.31 ± 0.02	0.69 ± 0.02	172 ± 16[c]			0.37 ± 0.02	0.63 ± 0.03	260 ± 15		
60	0.35 ± 0.02	0.64 ± 0.02	217 ± 33			0.35 ± 0.03	0.65 ± 0.03	255 ± 19		
70	0.43 ± 0.03	0.55 ± 0.03	238 ± 21			0.59 ± 0.05	0.41 ± 0.05	267 ± 20		

[a] The slow component of the β_{2d}-modulated channel was identified only in I_{Ca} of high amplitude around the peak current.
[b] Relative size of the slow component of I_{Ca} through the β_2CED-modulated channel decreased with an increase of V_t from −20 to 0 mV.
[c] $p < 0.01$ compared to τ_f for β_2CED (unpaired t test).

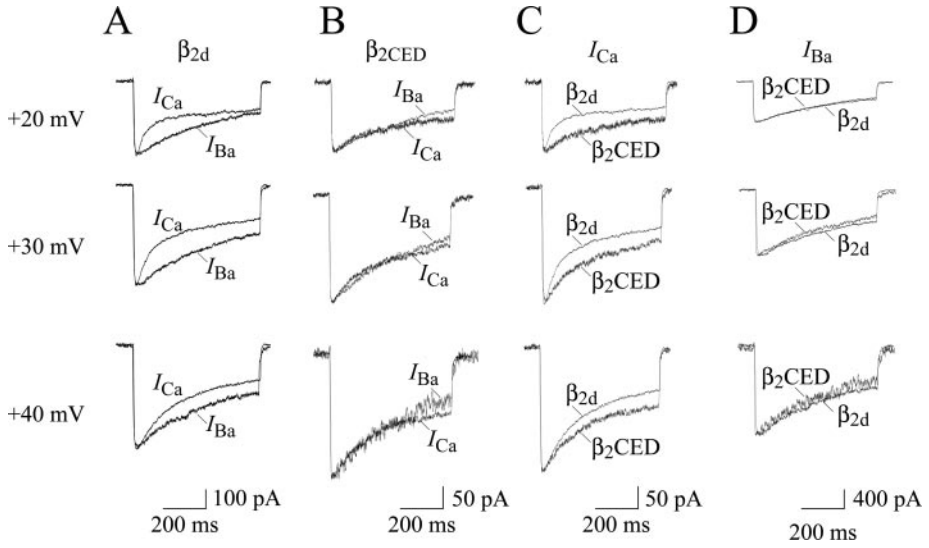

FIGURE 6. **Comparison of inactivation of the β_2CED- and β_{2d}-modulated calcium channels with Ca^{2+} and Ba^{2+} as the charge carrier.** *A* and *B*, comparison of I_{Ca} and I_{Ba} recorded from COS1 cells expressing $\alpha_{1C,77}/\alpha_2\delta$ and β_{2d} (*A*) or β_2CED (*B*). Current traces were normalized to the maximum amplitude of the respective I_{Ca}. One can see that I_{Ca} inactivated much faster than I_{Ba} in the case of β_{2d}, but not β_2CED, thus confirming that β_2CED does not support CDI. *C* and *D*, comparison of I_{Ba} (*C*) and I_{Ca} (*D*) through the $\alpha_{1C,77}/\alpha_2\delta$ channels modulated by β_2CED or β_{2d}. The traces were normalized to the maximum amplitude of I_{Ca} through the $\alpha_{1C,77}/\alpha_2\delta/\beta_2$CED (*C*) and $\alpha_{1C,77}/\alpha_2\delta/\beta_{2d}$ (*D*) channels. Unlike CDI, voltage-dependent inactivation of the channel supported by β_2CED was not markedly changed. Currents were recorded at $V_t = +20$, +30, and +40 mV applied from $V_h = -90$ mV.

Having revealed these unusual inactivation properties of the β_2CED channel, we tested for CDI by calculating the f factor (31), which is the difference between the r_{50} values, or fractions of I_{Ca} and I_{Ba} remaining at the end of a 50-ms depolarization. The 50-ms window was selected to accurately account for the relatively fast decay of I_{Ca} in the range of −20 to +10 mV (Fig. 5*A*). Confirming the result of the τ-V analysis (Fig. 5*D*), no U-shaped dependence of r_{50} on V_t was observed for I_{Ca}, whereas those for I_{Ba} was almost flat (Fig. 5*F*). A sharp difference between r_{50} values for I_{Ba} and I_{Ca} at lower voltages reflects a switch from an apparent biexponential voltage-dependent inactivation at −20 to 0 mV to a predominantly single-component mechanism at $V_t \geq 10$ mV (see above). One could argue that this result may be due to a specific level of intracellular Ca^{2+} buffering in our experiment. However, CDI in $Ca_v1.2$ calcium channels exhibits low sensitivity to intracellular Ca^{2+} buffers (32, 33). The possibility that β_2CED evokes CDI only in the narrow voltage range of −20 to 0 mV is doubtful because Ca^{2+} currents at these potentials are relatively small, and contribution of the voltage-dependent inactivation is probably greater. Making no further assumptions about the nature of this property, we compared inactivation of I_{Ca} and I_{Ba} near the maximum of I-V curves (Fig. 5, *D* and *E*), where CDI should be the most prominent (30). The difference f between r_{50} values at +30 to +50 mV was close to zero ($f = 0.04 \pm 0.02$ at +40 mV, Fig. 5*F*). This result is consistent with the lack of CDI and explains the slow kinetics of I_{Ca} decay in the β_2CED channel by the lack of the negative feedback regulation of inactivation by the permeating Ca^{2+} ions.

Overlaying of I_{Ca} and I_{Ba} traces, scaled to the same amplitude, is a common approach to estimate the contribution of CDI and voltage-dependent mechanisms in inactivation of the channel. In Fig. 6 we compared inactivation properties of β_2CED- and β_{2d}-modulated channels by superimposing I_{Ca} and I_{Ba} traces near the maximum of I-V curves. At V_t between +20 and +40 mV, where the currents are larger, the β_{2d}-modulated I_{Ca} inactivated notably faster than I_{Ba} (Fig. 6*A*) due to CDI. In contrast, we observed a matching decay of I_{Ca} and I_{Ba} for the β_2CED-modulated channel (Fig. 6*B*) confirming the lack of CDI. We next compared decays of I_{Ca} and I_{Ba} sampled near the maximum of I-V curves. Because of CDI, the β_{2d}-modulated I_{Ca} inactivated appreciably faster than with β_2CED (Fig. 6*C*). However, I_{Ba} through both β_2CED- and β_{2d}-modulated channels recorded at the same test voltages showed a very similar decay (Fig. 6*D*) indicating striking similarity of the voltage-dependent inactivation of the channels. Thus, the Ca^{2+}/Ba^{2+} test confirmed lack of CDI in the β_2CED-modulated channel. Lack of CDI is an unusual property that was not previously observed in $Ca_v1.2$ channels with native pore-forming α_{1C} subunits.

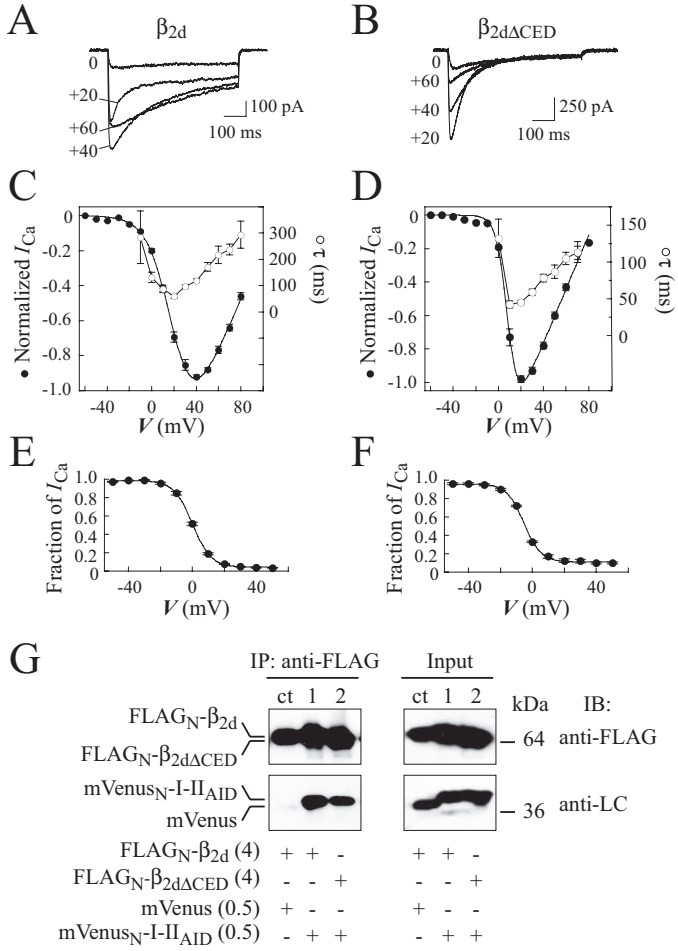

FIGURE 7. **Effect of the β_2CED deletion from β_{2d} on inactivation properties of the channel and binding to AID.** *A–F*, effect on I_{Ca}. COS1 cells were transfected with $\alpha_{1C,77}$, $\alpha_2\delta$, and ECFP$_N$-β_{2d} (*A, C,* and *E*) or ECFP$_N$-$\beta_{2d\Delta CED}$ (*B, D,* and *F*). *A* and *B,* exemplar traces of I_{Ca} evoked by the indicated test potentials applied for 600 ms from $V_h = -90$ mV. *C* and *D,* normalized *I-V* curves (*filled circles*) co-plotted with τ-*V* relations (*open circles*). Values of τ were obtained from single exponential fitting. β_{2d}, $V_{0.5,act} = 20.7 \pm 0.8$ mV, $n = 16$ (*C*). $\beta_{2d\Delta CED}$, $V_{0.5,act} = 8.5 \pm 0.5$ mV; $n = 12$ (*D*). *E* and *F,* steady-state inactivation curves. β_{2d}, $V_{0.5,in} = 0.1 \pm 0.2$ mV, $k_i = 5.8 \pm 0.1$, $n = 20$ (*E*). $\beta_{2d\Delta CED}$, $V_{0.5,in} = -5.3 \pm 0.3$ mV, $k_i = 5.3 \pm 0.2$, $n = 13$ (*F*). *Smooth lines* in *panels C–F* represent fits of the average data. *G,* deletion of β_2CED from β_{2d} does not interfere with binding to AID. FLAG$_N$-β_{2d} (*lanes ct* and *1*) or FLAG$_N$-$\beta_{2d\Delta CED}$ (*lane 2*) was co-expressed with mVenus (control, *lane ct*) or mVenus$_N$-I-II$_{AID}$ (*lanes 1* and *2*). Proteins were solubilized, immunoprecipitated with anti-FLAG Ab, and both the pre-IP (*input*) and IP fractions were resolved by SDS-PAGE (see "Experimental Procedures"). FLAG$_N$-tagged β_{2d} and $\beta_{2d\Delta CED}$ were identified on Western blot by anti-FLAG Ab (*top panels*). mVenus and mVenus$_N$-I-II$_{AID}$ were detected by anti-LC Ab (*bottom panels*). Molecular mass calibration in kDa is shown at the *right*. Amount of plasmid DNA (μg) per transfection reaction is given in *parentheses*. In the control assay, binding of mVenus to the tested Ca$_v\beta$ was not observed (*lane ct*).

Effect of β_2CED Deletion from β_{2d} on the Ca$_v$1.2 Calcium Channel—To better understand the functional impact of β_2CED on Ca$_v\beta_2$ subunit modulation of Ca$_v$1.2 channels, the distal 41-amino acid sequence (identical to those of $\beta_{2\Delta g}$(124–164)) was genetically deleted from β_{2d}. Modulation of the Ca$_v$1.2 channel by the obtained deletion mutant $\beta_{2d\Delta CED}$ was compared with those of β_{2d} (Fig. 7). Similar to other Ca$_v\beta$ subunits, β_{2d} facilitated large I_{Ca} through the Ca$_v$1.2 channel. Distinct features of I_{Ca} through the β_{2d} channel include: 1) a relatively large sustained component of the current that comprised ~35% of the peak current at the end of a 600-ms depolarization pulse (Fig. 7*A*), and 2) a prominent shift of the maximum *I-V* curve from a typical value of +20 to +30 mV (15) to +40 mV (Fig. 7*C*, *closed circles*). As expected, β_{2d} supported CDI and showed a U-shaped τ-*V* dependence of I_{Ca} peaked near the maximum of *I-V* curve (Fig. 7*C*, *open circles*).

The $\beta_{2d\Delta CED}$-modulated channel generated large inward I_{Ca} (average maximal amplitude 466 ± 160 pA, $n = 12$) in response to depolarization in a characteristic range of membrane potentials (Fig. 7*B*). Similar to the β_{2d}-modulated channel, decay of I_{Ca} at all tested potentials was better fitted by a single exponential. The τ-*V* relation had a distinct U-shape indicating that deletion of the β_2CED from the β_{2d} subunit did not compromise CDI (Fig. 7*D*). The maximal inactivation rate of I_{Ca} through the $\beta_{2d\Delta CED}$-modulated channel was faster ($\tau = 43 \pm 5$ ms at +10 mV) than that modulated by β_{2d} ($\tau = 59 \pm 6$ ms at +20 mV). The voltage dependence of activation ($V_{0.5,act}$) and inactivation ($V_{0.5,in}$) of the $\beta_{2d\Delta CED}$-modulated channel were shifted by ~12 (Fig. 7, *C* and *D*) and 5 mV (Fig. 7, *E* and *F*) to more negative voltages, respectively, suggesting that deletion of β_2CED endows the channel a higher voltage sensitivity (for statistics, see figure legend). Taken together, these results and data in Fig. 5 point to a synergy between MAGUK and β_2CED, but they may act independently as modulators of the Ca$_v$1.2 channel.

At present, the prevailing view suggests that AID is a constitutive binding site for all known Ca$_v\beta$ subunits. To further test whether deletion of β_2CED from the β_{2d} subunit interferes with binding to AID, we used the I-II$_{AID}$ peptide (amino acids 418–455 of the $\alpha_{1C,77}$ subunit) that harbors AID (amino acids 428–445) in its central part and retains binding affinity to Ca$_v\beta$ subunits (34). To ease IP and detection, I-II$_{AID}$ was tagged at the N terminus with the monomeric m*Venus* protein (29). The mVenus$_N$-labeled I-II$_{AID}$ was co-expressed with FLAG$_N$-tagged β_{2d} (Fig. 7*G*, *lane 1*) or $\beta_{2d\Delta CED}$ (*lane 2*) in HEK293 cells. Consistent with the results of electrophysiological experiments (Fig. 7, *A–F*), Western blot analysis of co-IP showed that deletion of CED from β_{2d} did not compromise binding of $\beta_{2d\Delta CED}$ to I-II$_{AID}$ as compared with β_{2d} (Fig. 7*G*).

*β_2CED Supports Ca$_v$1.2 Channels in the Absence of AID*—When mVenus$_N$-β_2CED and Biotin$_N$-I-II$_{AID}$ were co-expressed in HEK293 cells (Fig. 8*A*), β_2CED was identified (*lane 1*) on Western blot by monoclonal anti-LC Ab in both the immunoprecipitated (*top left panel*) and input (*top right panel*) fractions. However, I-II$_{AID}$ was detected on the blot by streptavidin only in the input fraction (*bottom panel*). Thus, co-IP analysis indicates that β_2CED does not bind to AID. These data suggest that β_2CED exerts its modulation of the Ca$_v$1.2 channel through interaction with a site(s) other than AID.

To confirm this conclusion, we abolished binding of the β subunit MAGUK domain to α_{1C} by the combined substitution with alanine at four key positions (Asp^{433}, Gly^{436}, Tyr^{437}, and Trp^{440}) of the α_{1C} I-II linker (10, 12, 35). Co-IP assay (Fig. 8*B*) confirmed that binding of β_{2d} to I-II$_{AID}$ (*lane 1*) was abolished by the AID mutation independently on the presence (*lane 2*) or absence (*lane 3*) of β_2CED. The AID mutation was then incorporated into the $\alpha_{1C,77}$ subunit, and the resulting mutant $\alpha_{1C,77AIDM}$ was co-expressed in COS1 cells with $\alpha_2\delta$ and β_{2d} (Fig. 8*C*), $\beta_{2d\Delta CED}$ (Fig. 8*D*), $\beta_{2\Delta g}$ (Fig. 8*E*), or β_2CED (Fig. 8*F*).

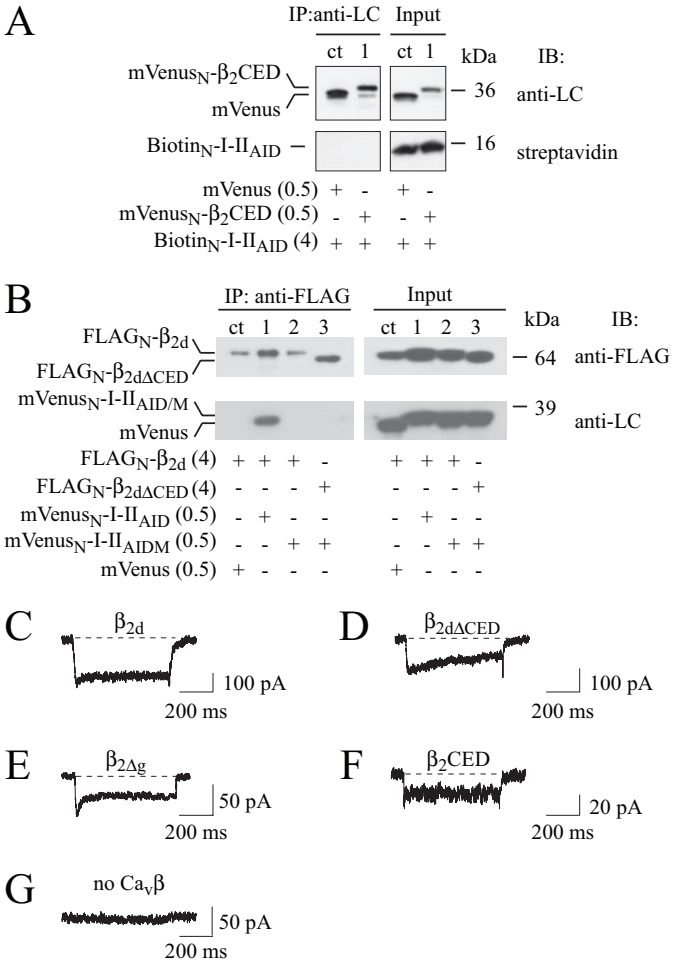

FIGURE 8. **Evidence that β_2CED does not target AID.** *A*, β_2CED does not bind to AID. mVenus (*control, lane ct*) or mVenus$_N$-β_2CED (*lane 1*) was co-expressed with Biotin$_N$-I-II$_{AID}$ in HEK293 cells. Proteins were immunoprecipitated (*IP*) with polyclonal anti-LC Ab and resolved by SDS-PAGE. mVenus (*ct*) and β_2CED (*1*) were identified on Western blot (*IB*) by monoclonal anti-LC Ab (*top panels*), whereas I-II$_{AID}$ was identified by streptavidin (*bottom panels*). *B,* combined mutation D433A,G436A,Y437A,W440A of I-II$_{AID}$ (I-II$_{AIDM}$; see "Experimental Procedures") inhibited binding of β_{2d}. Co-IP of mVenus (*ct*), mVenus$_N$-I-II$_{AID}$ (*lane 1*), or mVenus$_N$-I-II$_{AIDM}$ (*lanes 2* and *3*) with FLAG$_N$-β_{2d} (*lanes ct, 1* and *2*) or FLAG$_N$-$\beta_{2d\Delta CED}$ (*lane 3*) was assayed as described in the legend to Fig. 7*G*. The amount of plasmid DNA (μg) per transfection reaction is shown in *parentheses*. *C–G*, modulation of the $\alpha_{1C,77AIDM}$ channel current by β_{2d} (*C*), $\beta_{2d\Delta CED}$ (*D*), $\beta_{2\Delta g}$ (*E*), β_2CED (*F*), or no Ca$_v\beta$ (*G*) after co-expression with $\alpha_2\delta$ in COS1 cells. Shown are representative traces of maximal I_{Ca} recorded in response to a stepwise depolarization to +10 (*E*) or +30 mV (all other) applied for 600 ms from $V_h = -90$ mV.

Electrophysiological experiments showed that, despite the inhibited binding between MAGUK and AID (Fig. 8*B*), β_{2d} facilitated I_{Ca} through the mutated $\alpha_{1C,77AIDM}$ channel that showed little, if any, inactivation (Fig. 8*C*). As it is shown in Fig. 2*B*, no current could be detected in COS1 cells expressing $\alpha_{1C}/\alpha_2\delta$ in the absence of Ca$_v\beta$. The AID mutation did not inhibit conductance completely, but reduced the amplitude of the maximal I_{Ca} induced by β_{2d} to 131 ± 25 pA ($n = 5$) suggesting that the channel activation outside of AID by the full-size $Ca_v\beta_2$ does occur, but is less effective than that with the participation of intact AID. The same conclusion was obtained with $\beta_{2d\Delta CED}$, $\beta_{2\Delta g}$, and β_2CED. When β_{2d} was substituted for $\beta_{2d\Delta CED}$ (Fig. 8*D*), we observed a functionally active channel that exhibited a slowly inactivating I_{Ca} with an average maximum amplitude of

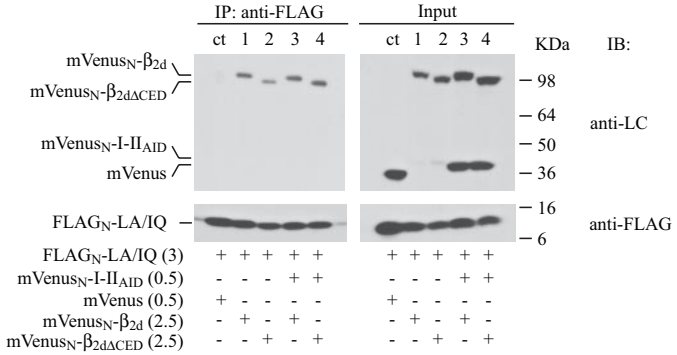

FIGURE 9. **Both β_{2d} and $\beta_{2d\Delta CED}$ bind to the LA/IQ domain independently on AID.** mVenus$_N$-β_{2d} (*lanes 1* and *3*) or mVenus$_N$-$\beta_{2d\Delta CED}$ (*lanes 2* and *4*) were co-expressed with FLAG$_N$-LA/IQ in the presence (*lanes 3* and *4*) or absence of mVenus$_N$-I-II$_{AID}$. *ct*, control showing lack of interaction between mVenus and FLAG$_N$-LA/IQ. *Upper panels*, identification of β_{2d}, $\beta_{2d\Delta CED}$, and I-II$_{AID}$ on Western blot by monoclonal anti-LC Ab. *Lower panels*, identification of LA/IQ by anti-FLAG Ab. Amount of plasmid DNA (μg) per transfection reaction is shown in *parentheses*. *IB*, immunoblot.

150 ± 24 pA ($n = 6$). Similar to $\beta_{2\Delta g}$ (Fig. 8*E*), inactivation of a large fraction of I_{Ca} was inhibited by substitution of β_{2d} for β_2CED (Fig. 8*F*), whereas the average amplitude of the peak I_{Ca} through the $\alpha_{1C,77AIDM}$ channel was smaller (40 ± 15 pA, $n = 3$). No appreciable modulation of the $\alpha_{1C,77AIDM}$ channel (*i.e.* zero I_{Ca}) was observed in the absence of Ca$_v\beta$ (Fig. 8*G*). Thus, inhibition of the MAGUK domain binding to AID did not abolish the sensitivity of the channel to β_2CED. These data confirm that essential regulatory properties of Ca$_v\beta$ are AID-independent (17) and show that β_2CED can serve as a weak I-II linker-independent activator of the Ca$_v$1.2 channel even when AID is mutated causing large conformational changes in the I-II loop.

Analysis of β_2CED Interaction with the LA/IQ Region of α_{1C}— A meaningful characterization of the β_2CED modulation of the channel requires identification of its functional target. A recent report (36) demonstrated that the N-terminal domain of MAGUK in Ca$_v\beta$ binds to the α_{1C} subunit C-terminal region (amino acids 1571–1636 in $\alpha_{1C,77}$) that is involved in CaM-mediated CDI regulation and includes LA and IQ loci of interaction with apo-CaM and Ca^{2+}/CaM, respectively (37) (Fig. 1). Because β_2CED does not support CDI, we tested β_{2d} (containing β_2CED) and $\beta_{2d\Delta CED}$ (lacking β_2CED) for binding to LA/IQ. Co-IP analysis showed (Fig. 9) that LA/IQ binds β_{2d} and $\beta_{2d\Delta CED}$ independently on the presence of I-II$_{AID}$; moreover, β_{2d} and $\beta_{2d\Delta CED}$ bound to LA/IQ do not form triple complexes with I-II$_{AID}$.

We then tested β_2CED for binding to LA/IQ. The FLAG$_N$-tagged LA/IQ domain was co-expressed with mVenus$_N$-β_2CED (Fig. 10) in the presence (*lanes 1* and *2*) or absence of ECFP$_N$-CaM (*lanes 3* and *4*). To assess for Ca^{2+} dependence of binding, cells were permeabilized for external Ca^{2+} before co-IP by incubating with ionophore ionomycin (5 μM) in the bath medium containing 2 mM EGTA (*lanes 1* and *3*) or 2 mM Ca^{2+} (*lanes 2* and *4*). Co-IP analysis confirmed that β_2CED binds to LA/IQ independently on Ca^{2+} or co-expressed CaM.

Is LA/IQ the only region necessary for β_2CED action? To answer this question, we deleted LA/IQ from the $\alpha_{1C,77}$ subunit and co-expressed the resulting $\alpha_{1C,77\Delta LK}$ mutant with $\alpha_2\delta$ and β_{2d} or β_2CED (Fig. 11*A*). β_{2d} modulated the channel via

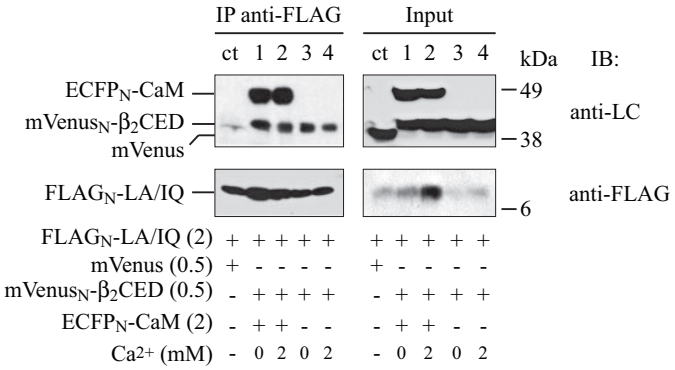

FIGURE 10. **β_2CED binds to LA/IQ domain independently on Ca^{2+} and CaM.** FLAG$_N$-LA/IQ was co-expressed with mVenus (control, *lane ct*) or mVenus$_N$-β_2CED (*lanes 1–4*) in the presence (*lanes 1* and *2*) or absence (*lanes 3* and *4*) of ECFP$_N$-CaM. Before co-IP, cells were incubated for 5 min in 10 mM HEPES, 150 mM NaCl (pH 7.4), containing 5 μM of ionomycin and either 2 mM EGTA (*lanes 1* and *3*) or 2 mM $CaCl_2$ (*lanes 2* and *4*). Proteins were co-IP with anti-FLAG Ab and resolved by SDS-PAGE. *Upper panels*, identification of CaM and β_2CED on Western blot by monoclonal anti-LC Ab (*lanes 1–4*). *Lower panels*, identification of LA/IQ by anti-FLAG Ab. The amount of plasmid DNA (μg) per transfection reaction is shown in *parentheses*.

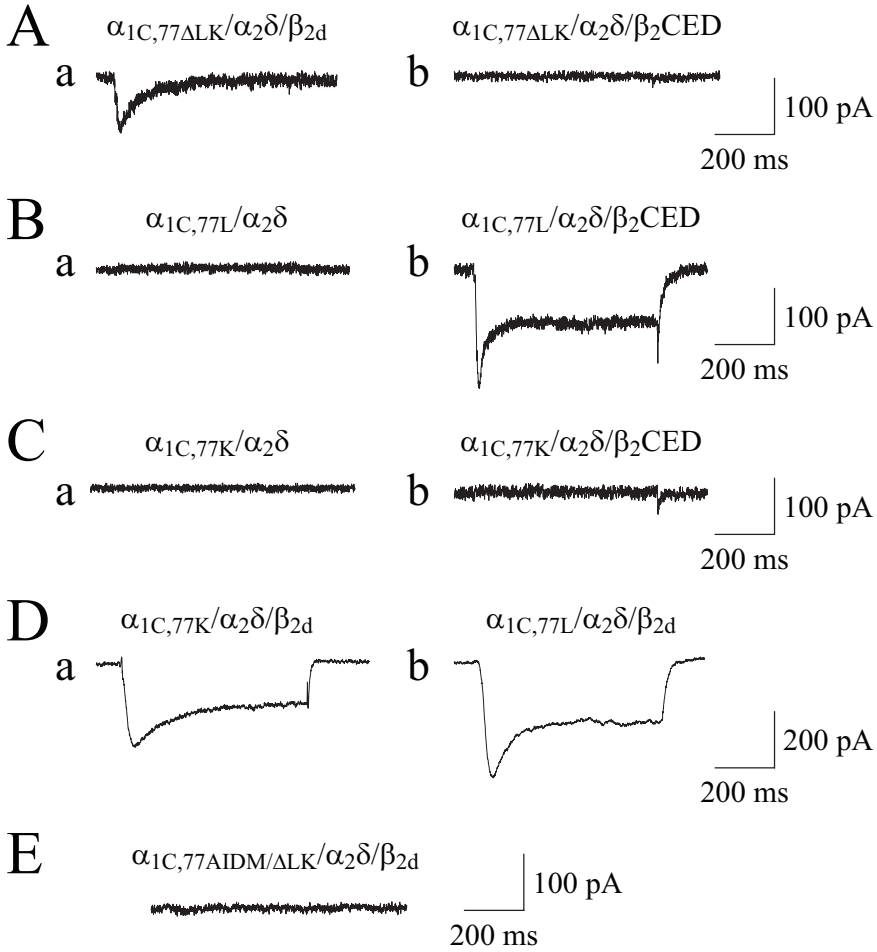

FIGURE 11. **Functional assessment of the role of LA/IQ in modulation of the Ca_v1.2 calcium channel by β_2CED.** *A*, deletion of LA/IQ from $\alpha_{1C,77}$ abolished facilitation of the $\alpha_{1C,77\Delta LK}$ channel I_{Ca} gating by β_2CED, but not by β_{2d}. $\alpha_{1C,77\Delta LK}$ was co-expressed in COS1 cells with $\alpha_2\delta$ in the presence of mVenus$_N$-β_{2d} (*panel a*) or mVenus$_N$-β_2CED (*panel b*). *B* and *C*, β_2CED supports gating of the IQ-mutated $\alpha_{1C,77L}$ channel but not the LA-mutated $\alpha_{1C,77K}$ channel. $\alpha_{1C,77L}$ (*B*) or $\alpha_{1C,77K}$ (*C*) was co-expressed in COS1 cells with $\alpha_2\delta$ in the absence (*panels a*) or presence (*panels b*) of mVenus$_N$-β_2CED. *D*, evidence that β_{2d} supported I_{Ca} in the $\alpha_{1C,77K}$ (*panel a*) and $\alpha_{1C,77L}$ (*panel b*) channels. *E*, simultaneous mutation of AID and deletion of LA/IQ abolished modulation of the $\alpha_{1C,77AIDM/\Delta LK}/\alpha_2\delta$ channel by β_{2d}. Shown are representative traces of maximal I_{Ca} recorded in response to a stepwise depolarization to +30 (*A* and *D*) or +20 mV (*B*, *C*, and *E*) applied for 600 ms from $V_h = -90$ mV.

MAGUK/AID interaction and induced I_{Ca} with an average maximal amplitude ~90 ± 25 pA (*panel a*, $n = 3$). Under the same conditions, with β_2CED no appreciable I_{Ca} was observed on cell depolarization (*panel b*). This result suggests that the LA/IQ region is the only functional target of the α_{1C} subunit where β_2CED may exert its action. To test whether LA or IQ determinants of CDI are essential for modulation of the channel by β_2CED, we examined the effect of β_2CED on the $\alpha_{1C,77}$ mutants lacking IQ (Fig. 11*B*, $\alpha_{1C,77L}$) or LA (Fig. 11*C*, $\alpha_{1C,77K}$) determinants defined in Fig. 1. In the absence of $Ca_v\beta$, none of the tested channels showed appreciable I_{Ca} in response to $V_t = +20$ mV applied from $V_h = -90$ mV for 600 ms (Fig. 11, *B* and *C*, *panels a*). Co-expression of β_2CED induced I_{Ca} only with $\alpha_{1C,77L}$ (average maximal amplitude ~208 ± 28 pA, $n = 5$, see Fig. 11*B*, *panel b*) indicating that it is the LA determinant of CDI that is the functional target of β_2CED modulation of the channel. Under the same conditions, β_{2d} supported I_{Ca} through both $\alpha_{1C,77K}$ (Fig. 11*D*, *panel a*; average maximal amplitude 231 ± 13 pA, $n = 14$) and $\alpha_{1C,77L}$ channels (Fig. 11*D*, panel b; average maximal amplitude 389 ± 24 pA, $n = 8$). However, mutation of AID combined with the deletion of LA/IQ from the α_{1C} subunit ($\alpha_{1C,77AIDM/\Delta LK}$) completely inhibited modulation of the channel by β_{2d} (Fig. 11*E*).

DISCUSSION

Our study revealed that modulation of Ca_v1.2 channels by large $Ca_v\beta_2$ subunits is mediated by inputs from multiple binding sites. There are at least three interactions between α_{1C} and $Ca_v\beta_2$ subunits (Fig. 12, *A–C*) that induce activity of the channel not only jointly, but also when any two of the interactions are disrupted by mutations of α_{1C}. The Ca_v1.2 channel modulation common to all large $Ca_v\beta$ subunits is supported by the binding of the central MAGUK domain to the AID site of the α_{1C} subunit I-II linker (4) (Fig. 12*A*). This interaction stabilizes the functional conformation of AID (and, respectively, the I-II linker), as well as provides specific orientation of the rigid core of $Ca_v\beta$ important for multiple isoform-specific interactions leading to differential modulation of the channel (15, 17). However, disruption of this interaction by the mutation of AID (Fig. 8*B*) does not prevent activation of the channel by $Ca_v\beta$ that relies on two other α_{1C} determinants located in the LA-IQ region (Figs. 5 and 8, *C*, *D*, and *F*). Deletion of these LA/IQ

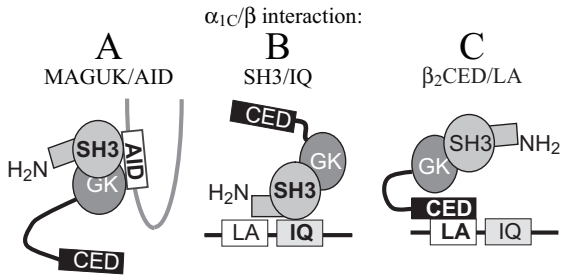

Channel	A	B	C	$I_{Ca}/I_{Ca}(\beta_{2d})$*	Fig.
$\alpha_{1C,77}/\alpha_2\delta/\beta_{2d}$	+	+	+	1.00	7*A*
$\alpha_{1C,77}/\alpha_2\delta/\beta_{2d\Delta CED}$	+	+	-	0.72	7*B*
$\alpha_{1C77,AIDM}/\alpha_2\delta/\beta_{2d}$	-	+	+	0.20	8*C*
$\alpha_{1C77,AIDM}/\alpha_2\delta/\beta_{2d\Delta CED}$	-	+	-	0.23	8*D*
$\alpha_{1C77,AIDM}/\alpha_2\delta/\beta_2$CED	-	-	+	0.06	8*F*
$\alpha_{1C,77}/\alpha_2\delta/\beta_2$CED	-	-	+	0.19	5
$\alpha_{1C,77AIDM/\Delta LK}/\alpha_2\delta/\beta_{2d}$	-	-	-	-	11*E*
$\alpha_{1C,77\Delta LK}/\alpha_2\delta/\beta_2$CED	-	-	-	-	11*A*(b)
$\alpha_{1C,77\Delta LK}/\alpha_2\delta/\beta_{2d}$	+	-	-	0.14	11*A*(a)
$\alpha_{1C,77L}/\alpha_2\delta/\beta_2$CED	-	-	+	0.32	11*B*(b)
$\alpha_{1C,77L}/\alpha_2\delta/\beta_{2d}$	+	-	+	0.60	11*D*(b)
$\alpha_{1C,77K}/\alpha_2\delta/\beta_2$CED	-	-	-	-	11*C*(b)
$\alpha_{1C,77K}/\alpha_2\delta/\beta_{2d}$	+	+	-	0.36	11*D*(a)

FIGURE 12. **Simplified diagrams of the three $Ca_v\beta_2/\alpha_{1C}$ interactions.** *A*, MAGUK/AID (4, 10–12); *B*, SH3/LA/IQ (36); *C*, β_2CED/LA. For clarity, potential interaction motifs are shown with sizes not to scale. Because the number of $Ca_v\beta$ per functional channel is not yet known, these schematic interactions are not unified into a single regulatory model. In the *lower part*, the mutated channels, implemented $Ca_v\beta_2/\alpha_{1C}$ interactions, relative size of I_{Ca} (*asterisk*) (normalized to those through the $\alpha_{1C,77}/\alpha_2\delta/\beta_{2d}$ channel) as well as references to the respective figure are listed.

determinants partially inhibited activity of the channel in the presence of β_{2d} as can be seen from the smaller I_{Ca} amplitude (Fig. 11*A*, *panel a*). A dynamic Ca^{2+}-dependent interaction between the N-terminal SH3 region of MAGUK and the IQ domain of the α_{1C} subunit (36) (Fig. 12*B*) appears to also be common to all large $Ca_v\beta$ subunits. This interaction alone is sufficient to support I_{Ca} (Fig. 8*D*).

In this study, we localized the third molecular determinant of the $Ca_v1.2$ channel modulation, β_2CED (Fig. 12*C*), which is specific only to $Ca_v\beta_2$ (Fig. 4) and resides in the C termini of β_{2a}, β_{2b}, β_{2c}, β_{2d}, β_{2e}, β_{2f}, and $\beta_{2\Delta g}$ subunits. Thus, β_2CED represents a functional element of the $Ca_v1.2$ modulation that is conserved in primary cardiac $Ca_v\beta_2$ subunits. In the case of full size $Ca_v\beta_2$ (β_{2a}-β_{2e}) (20), β_2CED acts in synergy with other determinants, as seen from the ability of β_2CED and $\beta_{2d\Delta CED}$ to support I_{Ca} with different properties (Figs. 5 and 7). However, β_2CED may induce activity of the channel independently on MAGUK, *i.e.* either alone (Fig. 5) or in the context of "short" β_2 subunits, as in the case of the naturally occurring $\beta_{2\Delta g}$ subunit (19) (Fig. 8*E*). Similar to other $Ca_v\beta$ subunits, β_2CED activates the channels by binding to α_{1C} (Fig. 3*F*) and targeting to PM (Fig. 3*E*), but does not support CDI (Fig. 5*D*). It appears that β_2CED affects voltage gating of the channel. Indeed, similar to β_{2d} (Fig. 7*C*), the β_2CED-modulated channel has the maximum *I-V* curve at +40 mV (Fig. 5*D*), whereas deletion of β_2CED from β_{2d} shifted the voltage dependence of I_{Ca} by 20 mV to lower potentials (Fig. 7*D*). We find that β_2CED binds to the LA/IQ region of the α_{1C} subunit C-terminal tail in a Ca^{2+}- and CaM-independent manner and needs the LA, but not IQ, motif to activate the channel (Fig. 10). This is the first observation of the $Ca_v\beta_2$ subunit regulation of the $Ca_v1.2$ calcium channel that does not rely on $Ca_v\beta$/AID interaction.

Although β_2CED did not bind to AID (Fig. 8*A*), mutation of AID interfered with the interaction of the channel with β_2CED that was reflected in the smaller amplitude of I_{Ca} (*cf.* Figs. 5*A* and 8*F*). This result points to high sensitivity of all three α_{1C}/$Ca_v\beta_2$ interactions (Fig. 12) to the conformation of AID that is probably a key component of mutually dependent determinants of channel regulation (7, 24).

Another important conclusion from our study is that CDI does not depend solely on the α_{1C} subunit. Indeed, co-expression of intact α_{1C} and $\alpha_2\delta$ subunits with β_2CED generates the channel lacking CDI (Figs. 5 and 6). It is known that CDI is mediated by interactions of CaM with two adjacent sites (LA and IQ) of the α_{1C} subunit C terminus (for review, see Ref. 38). We found that CDI ultimately requires both MAGUK/AID and SH3/IQ interactions (Fig. 12, *A* and *B*). Thus the role of $Ca_v\beta$, AID, and LA/IQ interactions in the ensemble of mutually coordinated determinants of CDI is essential.

The exact number of $Ca_v\beta$ subunits (of the same or different type) that bind to an individual α_{1C} subunit is unknown. Results in Fig. 9 show that β_{2d} is not involved in a simultaneous binding to LK and AID, although this subunit can be engaged in all three types of interactions shown in Fig. 12. Therefore, it is possible that there is more than one $Ca_v\beta_2$ subunit interacting with the same α_{1C}. On the other hand, if $Ca_v\beta$ does dissociate from the AID of the functional channel (39), then it is possible that modulation of the channel may be mediated by a single $Ca_v\beta_2$ molecule alternating between AID and LA/IQ sites. An additional complexity (36) to this general picture may be brought about by the N-terminal palmitoylation site known to anchor the β_{2a} subunit in PM (40).

Taken together, our results provide new insight into potential role(s) of β_2CED in modulation of $Ca_v1.2$ channels. $Ca_v\beta_2$ is a major cardiac β subunit and its splice variation is an important correlate of the $Ca_v1.2$ calcium channel regulation (20, 41). One of the most puzzling questions raised by our study is why $Ca_v\beta_2$ contains more than one α_{1C} interaction motif. One possible reason for this complexity may be associated with the role of β_2CED in additional tuning of the voltage dependence of the current (20). Indeed, results of electrophysiological measurements (Fig. 7) show that deletion of β_2CED from β_{2d} significantly changed kinetics of inactivation of I_{Ca} and shifted the peak of the *I-V* curve by 20 mV toward more negative potentials. Another reason may be that differential, tissue-specific splicing of the $Ca_v\beta_2$ gene (18) may generate subsets of the $Ca_v1.2$ calcium channel modulated only through β_2CED. These channels do not support CDI and generate small, but long-lasting Ca^{2+} currents. It is usually assumed that I_{Ca} is rapidly and fully inactivated, but our results raise the hypothesis that Ca^{2+} signaling in human cardiac cells expressing small $Ca_v\beta_2$ subunits (19) may involve Ca^{2+}-insensitive $Ca_v1.2$ channels in addition to L-type channels regulated by CDI. One possibility is that Ca^{2+} channels that rely on β_2CED-dependent, MAGUK-independent modulation in cardiac muscle cells may account

for the prolongation of L-type I_{Ca} and therefore contribute to the balance that controls the shape of the action potential plateau. Whichever role of β_2CED is predominant, it may be a new potential pharmacological target.

Acknowledgments—We thank Dr. S. S. Vogel (NIAAA, National Institutes of Health) for the gift of mVenus C1 plasmid, Dr. Kuanghueih Chen (NIA, National Institutes of Health) for the gift of pFLAG-2AB-pcDNA3, and Dr. Josephine Egan (NIA) for critically reading the manuscript.

REFERENCES

1. Jiang, Y., Lee, A., Chen, J., Cadene, M., Chait, B. T., and MacKinnon, R. (2002) *Nature* **417,** 523–526
2. Catterall, W. A. (2000) *Annu. Rev. Cell Dev. Biol.* **16,** 521–555
3. García, R., Carrillo, E., Rebolledo, S., García, M. C., and Sánchez, J. A. (2002) *J. Physiol.* (*Lond.*) **545,** 407–419
4. Pragnell, M., De Waard, M., Mori, Y., Tanabe, T., Snutch, T. P., and Campbell, K. P. (1994) *Nature* **368,** 67–70
5. Doyle, D. A., Morais Cabral, J., Pfuetzner, R. A., Kuo, A., Gulbis, J. M., Cohen, S. L., Chait, B. T., and MacKinnon, R. (1998) *Science* **280,** 69–77
6. Shi, C., and Soldatov, N. M. (2002) *J. Biol. Chem.* **277,** 6813–6821
7. Stotz, S. C., Jarvis, S. E., and Zamponi, G. W. (2004) *J. Physiol.* (*Lond.*) **554,** 263–273
8. Hanlon, M. R., Berrow, N. S., Dolphin, A. C., and Wallace, B. A. (1999) *FEBS Lett.* **445,** 366–370
9. Opatowsky, Y., Chomsky-Hecht, O., Kang, M.-G., Campbell, K. P., and Hirsch, J. A. (2003) *J. Biol. Chem.* **278,** 52323–52332
10. Chen, Y.-h., Li, M.-h., Zhang, Y., He, L.-l., Yamada, Y., Fitzmaurice, A., Shen, Y., Zhang, H., Tong, L., and Yang, J. (2004) *Nature* **429,** 675–680
11. Opatowsky, Y., Chen, C.-C., Campbell, K. P., and Hirsch, J. A. (2004) *Neuron* **42,** 387–399
12. Van Petegem, F., Clark, K. A., Chatelain, F. C., and Minor, D. L., Jr. (2004) *Nature* **429,** 671–675
13. Beurg, M., Sukhareva, M., Ahern, C. A., Conklin, M. W., Perez-Reyes, E., Powers, P. A., Gregg, R. G., and Coronado, R. (1999) *Biophys. J.* **76,** 1744–1756
14. Cens, T., Mangoni, M. E., Richard, S., Nargeot, J., and Charnet, P. (1996) *Pflügers Arch. Eur. J. Physiol.* **431,** 771–774
15. Kobrinsky, E., Kepplinger, K. J. F., Yu, A., Harry, J. B., Kahr, H., Romanin, C., Abernethy, D. R., and Soldatov, N. M. (2004) *Biophys. J.* **87,** 844–857
16. Dolphin, A. C. (2003) *J. Bioenerg. Biomembr.* **35,** 599–620
17. Maltez, J. M., Nunziato, D. A., Kim, J., and Pitt, G. S. (2005) *Nat. Struct. Mol. Biol.* **12,** 372–377
18. Foell, J. D., Balijepalli, R. C., Delisle, B. P., Yunker, A. M. R., Robia, S. L., Walker, J. W., McEnery, M. W., January, C. T., and Kamp, T. J. (2004) *Physiol. Genomics* **17,** 183–200
19. Harry, J. B., Kobrinsky, E., Abernethy, D. R., and Soldatov, N. M. (2004) *J. Biol. Chem.* **279,** 46367–46372
20. Colecraft, H. M., Alseikhan, B., Takahashi, S. X., Chaudhuri, D., Mittman, S., Yegnasubramanian, V., Alvania, R. S., Johns, D. C., Marban, E., and Yue, D. T. (2002) *J. Physiol.* (*Lond.*) **541,** 435–452
21. Soldatov, N. M., Bouron, A., and Reuter, H. (1995) *J. Biol. Chem.* **270,** 10540–10543
22. Carlsson, J., Drevin, H., and Axén, R. (1978) *Biochem. J.* **173,** 723–737
23. Xiang, C. C., Mezey, E., Chen, M., Key, S., Ma, L., and Brownstein, M. J. (2004) *Nucleic Acids Res.* **32,** e185
24. Kobrinsky, E., Tiwari, S., Maltsev, V. A., Harry, J. B., Lakatta, E., Abernethy, D. R., and Soldatov, N. M. (2005) *J. Biol. Chem.* **280,** 12474–12485
25. Berjukow, S., Döring, F., Froschmayr, M., Grabner, M., Glossmann, H., and Hering, S. (1996) *Br. J. Pharmacol.* **118,** 748–754
26. Kurejova, M., Uhrik, B., Sulova, Z., Sedlakova, B., Krizanova, O., and Lacinova, L. (2007) *Eur. J. Pharmacol.* **567,** 10–18
27. Meir, A., Bell, D. C., Stephens, G. J., Page, K. M., and Dolphin, A. C. (2000) *Biophys. J.* **79,** 731–746
28. Ravindran, A., Lao, Q. Z., Harry, J. B., Abrahimi, P., Kobrinsky, E., and Soldatov, N. M. (2008) *Proc. Natl. Acad. Sci. U.S.A.*, in press
29. Koushik, S. V., Chen, H., Thaler, C., Puhl, H. L., III, and Vogel, S. S. (2006) *Biophys. J.* **91,** L99–101
30. Zhou, J., Olcese, R., Qin, N., Noceti, F., Birnbaumer, L., and Stefani, E. (1997) *Proc. Natl. Acad. Sci. U. S. A.* **94,** 2301–2305
31. Peterson, B., Lee, J., Mulle, J., Wang, Y., de Leon, M., and Yue, D. (2000) *Biophys. J.* **78,** 1906–1920
32. Cens, T., Restituito, S., Galas, S., and Charnet, P. (1999) *J. Biol. Chem.* **274,** 5483–5490
33. Liang, H., DeMaria, C. D., Erickson, M. G., Mori, M. X., Alseikhan, B. A., and Yue, D. T. (2003) *Neuron* **39,** 951–960
34. Takahashi, S. X., Miriyala, J., Tay, L. H., Yue, D. T., and Colecraft, H. M. (2005) *J. Gen. Physiol.* **126,** 365–377
35. Seu, L., and Pitt, G. S. (2006) *J. Gen. Physiol.* **128,** 605–613
36. Zhang, R., Dzhura, I., Grueter, C. E., Thiel, W., Colbran, R. J., and Anderson, M. E. (2005) *FASEB J.* **19,** 1573–1575
37. Romanin, C., Gamsjaeger, R., Kahr, H., Schaufler, D., Carlson, O., Abernethy, D. R., and Soldatov, N. M. (2000) *FEBS Lett.* **487,** 301–306
38. Morad, M., and Soldatov, N. (2005) *Cell Calcium* **38,** 223–231
39. Gerster, U., Neuhuber, B., Groschner, K., Striessnig, J., and Flucher, B. E. (1999) *J. Physiol.* (*Lond.*) **517,** 353–368
40. Qin, N., Platano, D., Olcese, R., Costantin, J. L., Stefani, E., and Birnbaumer, L. (1998) *Proc. Natl. Acad. Sci. U. S. A.* **95,** 4690–4695
41. Hullin, R., Khan, I. F. Y., Wirtz, S., Mohacsi, P., Varadi, G., Schwartz, A., and Herzig, S. (2003) *J. Biol. Chem.* **278,** 21623–21630